ACS APPLIED MATERIALS & INTERFACES

Research Article

www.acsami.org

Effects of Pulsing and Interfacial Potentials on Tellurium–Organic Heterostructured Films

Robert M. Ireland,[†] Thomas J. Dawidczyk,[†] Patrick Cottingham,[‡] Tyrel McQueen,[‡] Gary Johns,[§] Nina Markovic,[§] Lushuai Zhang,[§] Padma Gopalan,[§] and Howard E. Katz*,[†]

[†]Department of Materials Science and Engineering and Department of Chemistry, Johns Hopkins University, 3400 North Charles Street, Baltimore, Maryland 21218, United States

[‡]Department of Chemistry and Department of Physics and Astronomy, Johns Hopkins University, 3400 North Charles Street, Baltimore, Maryland 21218, United States

[§]Department of Physics and Astronomy, Johns Hopkins University, 3400 North Charles Street, Baltimore, Maryland 21218, United States

[§]Department of Materials Science and Engineering, University of Wisconsin, Madison, Wisconsin 53706, United States

Supporting Information

ABSTRACT: Polycrystalline thin films of tellurium and organic semiconductor molecules are paired in heterostructured field-effect transistors built on Si/SiO_2 substrates. While charge carrier mobilities can exceed 1 $cm^2/(V\ s)$, there is only a limited gate voltage range over which the current is modulated. We employ continuous and pulsed measurements on transistors to explore the influence of charge equilibration time on device behavior, finding that pulsed gating improves output characteristics. We also use surface potential measurements to investigate the interfacial vacuum level offset between materials, and we modify the interlayer potential profile by interposing statically charged dielectric layers on the silicon dioxide. We show that interfacial fields determine the gate voltage range over which Te shows a field effect in heterostructures with organic semiconductors and that modification of these fields can extend this range.

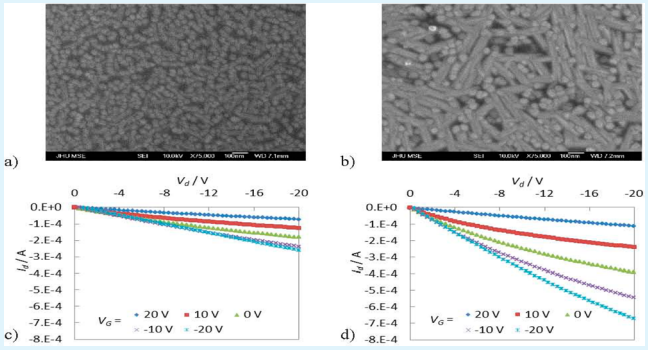

KEYWORDS: *organic electronics, tellurium, field-effect transistors, pulsed gating, interfacial potential differences, azo dye monolayers*

INTRODUCTION

Organic field-effect transistors (OFETs) comprise a gate electrode supplying gate voltage V_g, a gate dielectric, a semiconducting film typically of 10–100 nm thickness in which a charge channel forms, and source/drain electrodes between which current I_d flows, driven by drain voltage V_d. OFETs are now considered for display driver, sensor, and identification circuits[1−4] and are associated with complex electronic functionality, simple processing, transparency, and mechanical flexibility. These advantages could be realized from inorganic semiconductors as well, in the form of easily deposited films and nanostructures.[5−8] In a recent study, we described vapor-deposited elemental tellurium (Te) films with a wide variety of morphologies on differing substrates.[9] In particularly favorable cases, with Te deposited on an organic semiconductor (OSC), charge carrier (hole) mobility (μ) was >3 $cm^2\ V^{-1}\ s^{-1}$. However, this μ coincided with mostly depletion-regime activity, loss of field effect once reaching the accumulation regime, and poor saturation at high depletion voltages.

To better understand the reasons for these field effect behaviors, we now investigate local static electric fields spontaneously formed at the Te–organic interfaces and effects of intentional static charge implantation. We consider Te as an inorganic nanostructured semiconductor[13−18] on top of organic semiconductors pentacene or 5,5′-bis(4-hexylphenyl)-2,2′-bithiophene (6PTTP6).[19−21] We perform device characterization by conventional continuous voltage application and by pulsing V_g at 1 kHz. At this time scale, the equilibrium charge distribution is not always reached, and thus it is shown that field effect behavior can be enhanced at higher frequency. We also employ scanning Kelvin probe microscopy[24] to observe interfacial potential differences and use a statically charged gate dielectric[23] to alter those interfacial potentials. We show that V_g at which the field effect is lost is significantly influenced by internal fields.

Received: October 4, 2012
Accepted: February 13, 2013
Published: February 13, 2013

   dx.doi.org/10.1021/am302221h | *ACS Appl. Mater. Interfaces* 2013, 5, 1604–1611

Table 1. FET Parameters and Performance

semiconductor	dielectric	gate bias	μ_{meas} [$cm^2\ V^{-1}\ s^{-1}$][a]	V_T [V][a]	on/off	N_s[b]
6PTTP6[c]	SiO_2	pulsed[d]	0.028 ± 0.002	−3.29 ± 0.29	4230 ± 70	8
		static	0.025 ± 0.002	−1.97 ± 0.31	1840 ± 40	8
pentacene[c]	SiO_2	pulsed	0.053 ± 0.006	−4.60 ± 0.25	21000 ± 1400	4
		static	0.038 ± 0.001	−4.00 ± 0.35	1400 ± 400	4
Te	SiO_2	pulsed	1.7 ± 0.5	42.0 ± 0.8	3.38 ± 0.09	4
		static	1.10 ± 0.06	61.6 ± 2.0	2.08 ± 0.03	4
Te/6PTTP6	SiO_2	pulsed	1.55 ± 0.04	39.1 ± 1.1	4.30 ± 0.22	20
		static	0.82 ± 0.02	52.2 ± 1.5	2.85 ± 0.10	20
Te/pentacene	SiO_2	pulsed	2.7 ± 0.3	110 ± 6	1.8 ± 0.08	4
		static	1.4 ± 0.2	150 ± 10	1.5 ± 0.05	4

[a]Mobility, μ_{meas}, and V_T values were extrapolated from $I_d^{1/2}$ vs V_g plots. W/L is 80. [b]N_s is number of samples corresponding to calculated values and standard deviations. [c]Devices measured in the accumulation regime (V_g of 0 to −20 V). Te devices were analyzed in the depletion regime (V_g of 20 to 0 V). [d]Gate voltage was applied in pulses at 1 kHz. Static gate voltage was applied under DC.

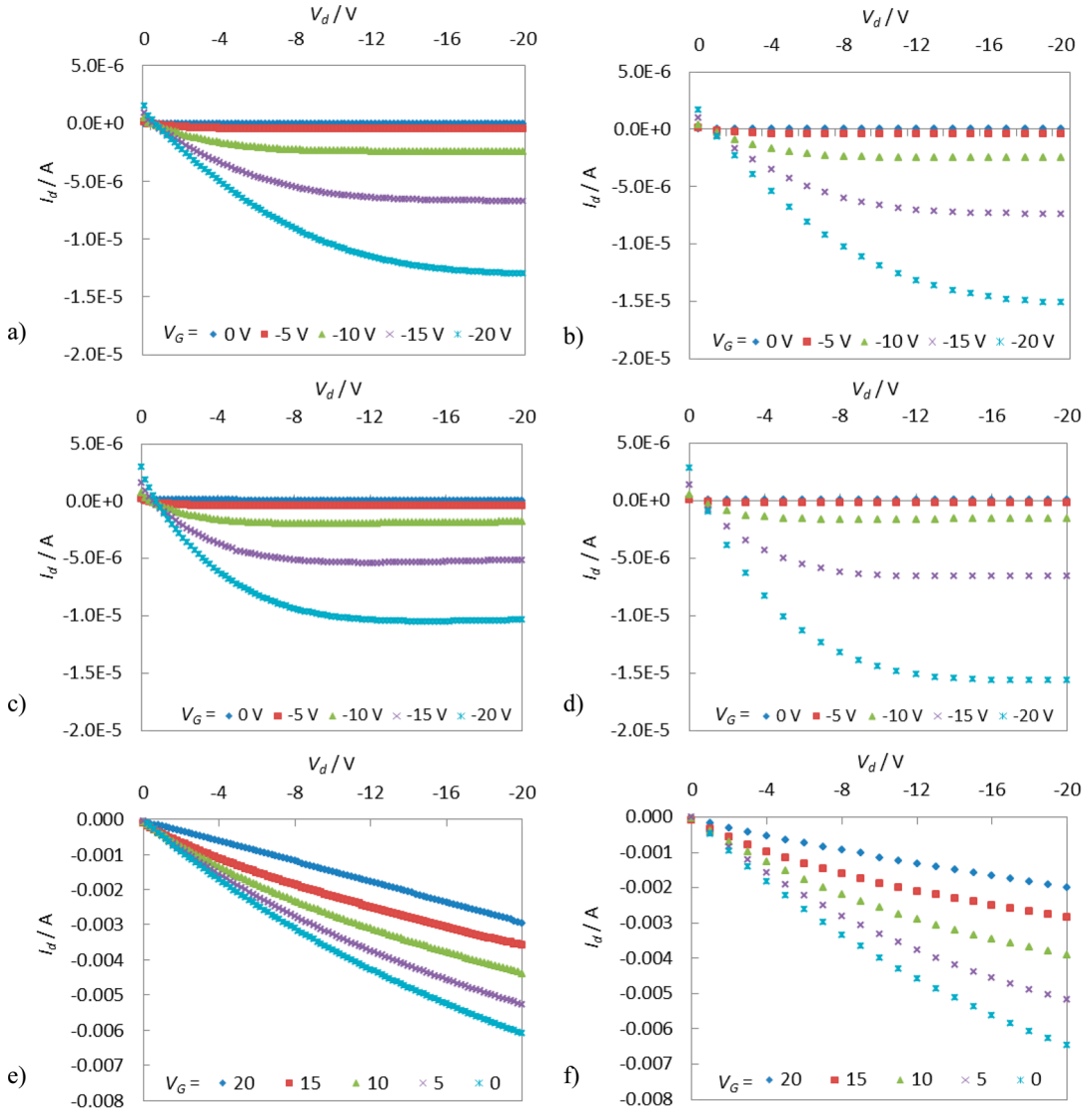

Figure 1. I_d vs V_d plots for (a) 6PTTP6/SiO_2 with static V_g and (b) V_g pulsed at 1 kHz. (c) Pentacene/SiO_2 with static V_g and (d) V_g pulsed at 1 kHz. (e) Te/SiO_2 with static V_g and (f) V_g pulsed at 1 kHz. V_g are shown in legends.

The field-effect charge carrier mobility μ is generally assumed to apply to the entire semiconductor film. Sometimes μ is acknowledged to be dependent on the electric field (gate voltage per unit dielectric thickness, V_g/d) applied across the gate dielectric between the gate electrode and semiconductor.[10] If traps in the semiconductor are filled as V_g increases, μ increases with V_g. It is also conceivable that higher V_g can drive the channel of mobile charge carriers from a high-μ bulk region of the semiconductor into a more disordered region of the semiconductor film within 2−5 nm (1−2 molecular mono-

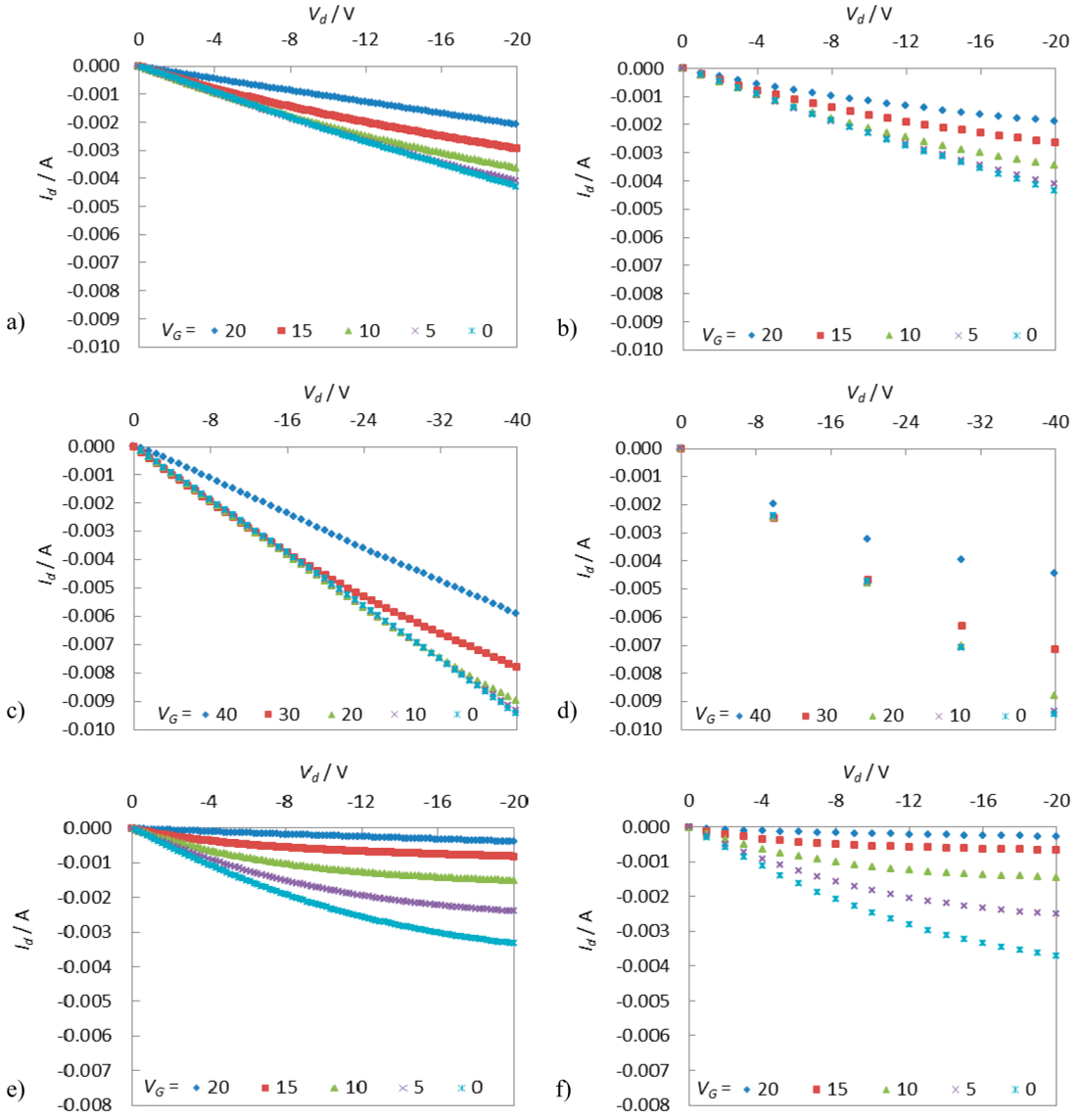

Figure 2. I_d vs V_d plot for (a) Te/6PTTP6/SiO_2 with static V_g and (b) V_g pulsed at 1 kHz. (c) Te/pentacene/SiO_2 with static V_g and (d) V_g pulsed at 1 kHz. (e) 6PTTP6/Te/6PTTP6/SiO_2 with static V_g and (f) V_g pulsed at 1 kHz.

layers) of the gate dielectric, in which case mobility would decrease as V_g increases.[11]

The dependence of μ on the device characterization time scale is rarely considered. Because of the RC time constant of a device test circuit, charge distribution in the semiconductor might not be at the equilibrium expected from the applied voltages. We recently used time-resolved measurements to characterize an OFET containing a fluoroalkylbenzyl-substituted naphthalenetetracarboxylic diimide (NTCDI) on a 3 nm oxide, showing that μ was higher on shorter time scales than on longer time scales, and some of the NTCDI layers closer to the gate dielectric contributed to gate capacitance.[12] This would have been consistent with the charge channel forming farther from the gate dielectric and in a higher mobility region compared to direct current (DC, "zero frequency") conditions.

Shifting of OSC energy levels at organic/organic[26−29] and organic/metal[29−31] junctions has been extensively investigated. However, a general model for these interfaces has not yet been accepted due to the wide variety of organic molecules and their ranges of impurity concentrations, mobilities, dielectric constants, densities of states at particular energies, ionization energies, and electron affinities. At junctions between weakly interacting OSCs, vacuum level alignment is expected. Between interfaces with greatly differing ionization energies or electron affinities, charge transfer tends to cause the formation of a "built-in" electrical potential (interface dipole) on the order of several tenths of an electronvolt. Fermi energy pinning often results from alignment of OSC energy levels with the work functions of metals, specifically at the interface, and the barrier height to charge transfer is expected to grow or shrink according to vacuum level shifting and voltage biasing between electrodes. However, the behavior of organic/inorganic semiconductor junctions can be less predictable and requires detailed case-by-case investigation.[5−8,15−18,32−35]

RESULTS AND DISCUSSION

Effect of Pulsing on Organic and Te FETs. Table 1 shows a comparison of device parameters for the three main individual materials of this study and the Te/OSC bilayers, all deposited at ambient temperature on SiO_2−Si substrates. Parameters for devices made from other combinations and

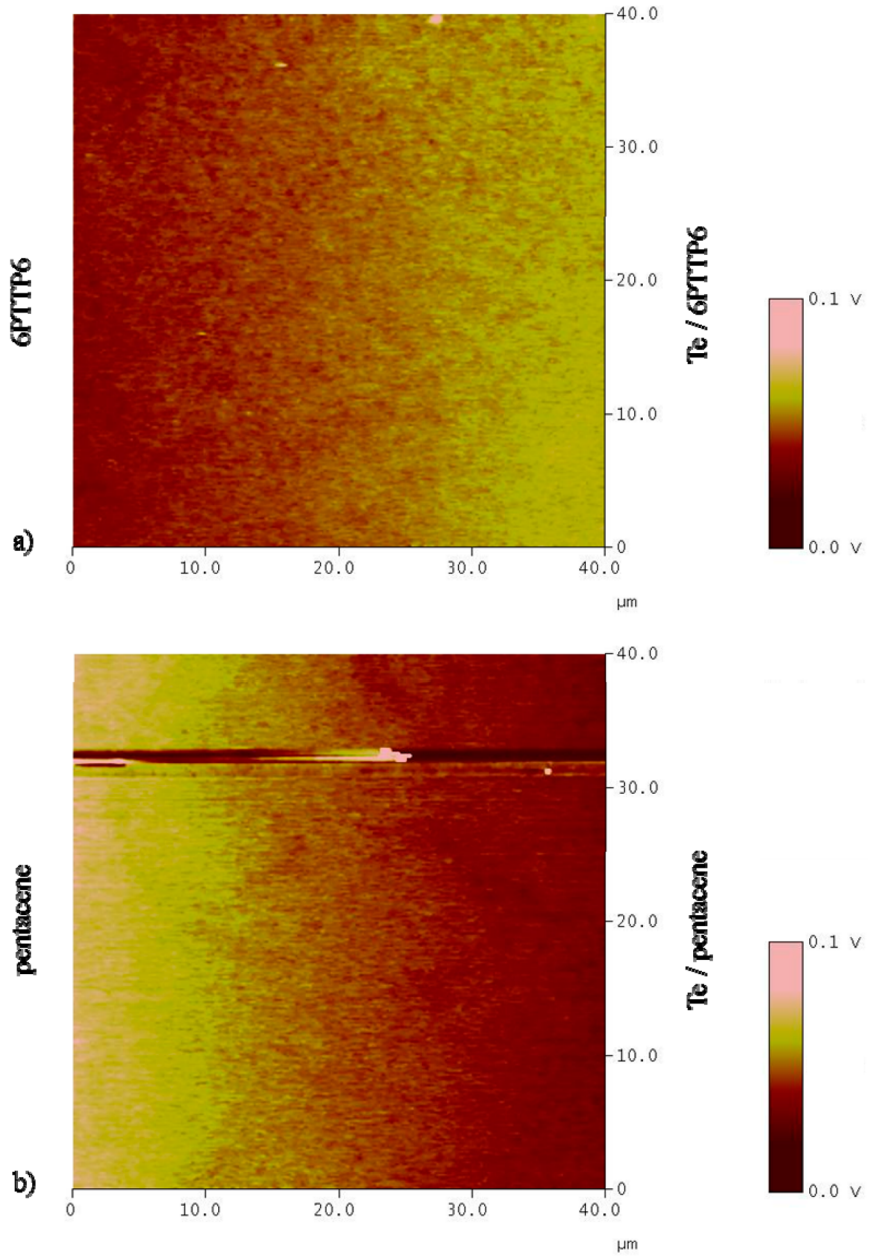

Figure 3. SKPM 2D surface potential scans of (a) 6PTTP6 vs Te/6PTTP6 from left to right and (b) pentacene vs Te/pentacene from left to right.

under other conditions are provided in the Supporting Information (Tables S1 and S2). Figure S1 (Supporting Information) portrays molecular structures for each material. Single material mobilities were as expected for the deposition conditions and were slightly increased, but not outside the range of statistical uncertainty, when data were collected at 1 kHz instead of under DC conditions, as seen qualitatively in the output characteristics shown in Figure 1. In particular, the Te plots are more spread and more curved at the most positive V_g.

When Te was deposited on either of the two OSCs, the field effect was lost in the accumulation regime, as we had previously observed. Field effect was lost in Te–6PTTP6 bilayers at V_g between +5 and +0 V, and in Te–pentacene bilayers between +20 and +10 V. Figure 2 shows the characteristics. While pulsing again improved the saturation behavior at the most positive V_g, doubling the apparent mobility and decreasing V_t, it had little effect on the accumulation regime. V_t of the Te devices, though remaining in the depletion regime, was shifted significantly toward the accumulation regime, suggesting that 1 ms was insufficient time to activate all of the extrinsic charges for collection.

Interfacial Fields in Te–Organic Heterostructures. To help explain the 10–15 V difference in field effect ranges between Te/6PTTP6 and Te/pentacene bilayers and the reason for field effect loss altogether, we performed scanning Kelvin probe microscopy (SKPM) on lateral boundaries at the interface between the bilayer materials deposited side-by-side. SKPM measures local variations in surface potential across an interface by scanning the junction at some distance above the surface (200 nm in this case) and then retraces the height profile while measuring changes in potential.[24] Here, SKPM qualitatively reveals the surface potential difference between a single 6PTTP6 layer and Te deposited onto 6PTTP6 as a bilayer and between a single pentacene layer and Te/pentacene.

Due to the limitations of shadow masks in our fabrication process, quantification of the potential difference spanning an entire sample was not possible because the diffuse interface is wider than the maximum scan length of our instrument (~40 μm) by a factor of 2−3. Regardless, the relative polarities on either side of the interfaces were clearly demarcated.

The results are shown in Figure 3, which indicate potential differences of opposite sign for 6PTTP6 and pentacene relative to Te on those OSCs. 6PTTP6 has more negative surface potential than Te deposited thereon. This indicates that holes are more stable in Te relative to 6PTTP6. Conversely, SKPM scans show pentacene with more positive surface potential than Te/pentacene. Therefore, pentacene more readily accepts holes from (donates electrons to) Te at equilibrium. This is consistent with the relative energy band compositions (Figure 4). The highest occupied molecular orbital (HOMO) and

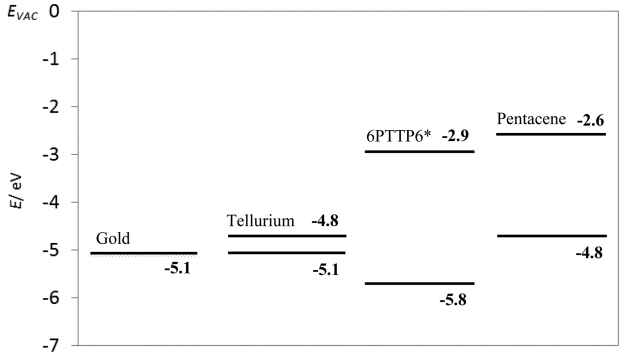

Figure 4. Work function of gold is shown relative to conduction and valence energy levels of tellurium (ref 14), HOMO/LUMO of 6PTTP6 (*estimated from dihexylquaterthiophene, ref 22), and HOMO/LUMO of pentacene (ref 19).

lowest unoccupied molecular orbital (LUMO) values of 6PTTP6 are estimated as those reported for 2,5-dihexylterthiophene,[22] which is expected to be slightly more electron donating than 6PTTP6. A consequence of the Te/6PTTP6 interfacial voltage is the stabilization of holes in the Te layer of a 6PTTP6/Te/6PTTP6 trilayer, which had the highest μ of the useful heterostructures from our previous study, as much as 3−5 cm^2/(V s) with Te deposited on a heated substrate.

The measured potentials are also consistent with losing field-effect in hybrid FETs at more positive V_g for Te/pentacene than Te/6PTTP6. The energy level change on driving holes from the source through the Te into the organic is lower for pentacene than for 6PTTP6, so given the lower mobilities of the OSCs relative to Te, the increase of source-drain conductance resulting from making V_g less positive ends at a more positive V_g with pentacene.

Effect of Static Charge in the Underlying Dielectric. We performed another experiment, this time aiming to alter the internal potentials determining the voltage at which the field effect is lost. We took advantage of our already reported technique of applying static charge to a nonpolar polymer dielectric,[20,21] in this case polystyrene[23] (PS), to shift OFET V_t, a method particularly effective for a normally off OSC such as 6PTTP6. Morphologies of Te structures deposited for this experiment are shown in Supporting Information Figures S2−S4.

Figure 5 shows characteristics of OFETs with 6PTTP6 and Te FETs using PS gate dielectric interlayers, with and without prior static charging of +50 V. This charging polarity would be expected to result in FETs with the off state shifted further into the accumulation regime.[22] Indeed, this was observed for 6PTTP6 alone (Figures 5a,b), with maintenance of the expected mobility, correcting for the lowered gate capacitance. Surprisingly, this charging turned Te-containing FETs more "on"; i.e., threshold voltage was shifted into depletion, and output current was increased (Figures 5c−f). Furthermore, compared to Figure 2a, the field effect of Te on 6PTTP6 extended farther into the accumulation regime with the polystyrene interlayer than without it, possibly reflecting the higher V_d needed to create the same gate field with the PS present. Static charging extends the field effect more significantly into accumulation, even though the charge density indicated by Figure 5f is also greater.

Thus, the polystyrene layer and the static charging both decrease the effective gate field that drives holes from Te into the 6PTTP6. The resulting increase in the V_g range showing a field effect is evidence for our hypothesis that the loss of field effect in uncharged devices is due to charge becoming more distributed in the lower-μ layer at more negative V_g, and not because of the more negative V_g eventually causing all hole-supporting sites in the Te to become filled. OFET performances for experiments on statically charged samples are summarized in the Supporting Information (Table S2). As was the case with Te on SiO_2, 1 kHz pulsing further spread the I_d-V_d curves, increasing the apparent mobility and lowering V_t.

Figure 6 shows schematic charge distributions for the two Te bilayers and for Te/6PTTP6 on charged polystyrene, before application of V_g. For the bilayers, the charge distributions reflect the relative stability of holes in the materials as indicated by SKPM. As discussed above, holes are more easily driven into pentacene by a negative gate voltage, lowering the mobility at a less negative V_g. For the charged system, the injected static charges are in the polystyrene, and some of those static charges act as remote dopants for the Te layer as well, though we do not expect that charges in the polystyrene are themselves mobile. The static charges pose a barrier to driving positive charges into the 6PTTP6, increasing the V_g range for useful field effect.

A particularly dramatic effect of pulsing is shown in Figure 7 for the system we had identified in our previous study as having the most conventional field effect behavior, Te deposited on a monolayer of azo dye (DR19) heated to 55 °C. V_t is brought to the accumulation regime because this dye adds traps to the dielectric surface, but at the expense of mobility relative to the unheated Te or Te on a bare substrate. Pulsing doubled the mobility compared to the DC measurement, consistent with charges not equilibrating with traps on the 1 kHz time scale, while the accumulation-only nature of the device was maintained. Thus, like in the above bilayer examples, pulsing placed charges preferentially in regions with higher mobility. In the DR19 case, the effect was from an increase in output current of a better behaved transistor, rather than simply extending the range over which current was modulated in depletion mode.

SUMMARY AND CONCLUSIONS

The apparent quality of Te-based FETs is shown to depend on both the time scale of the measurement (1 kHz vs DC) and internal potential differences among layers of which the devices are comprised. Te serves as a useful test platform for inorganic−organic heterostructures because of its high mobility

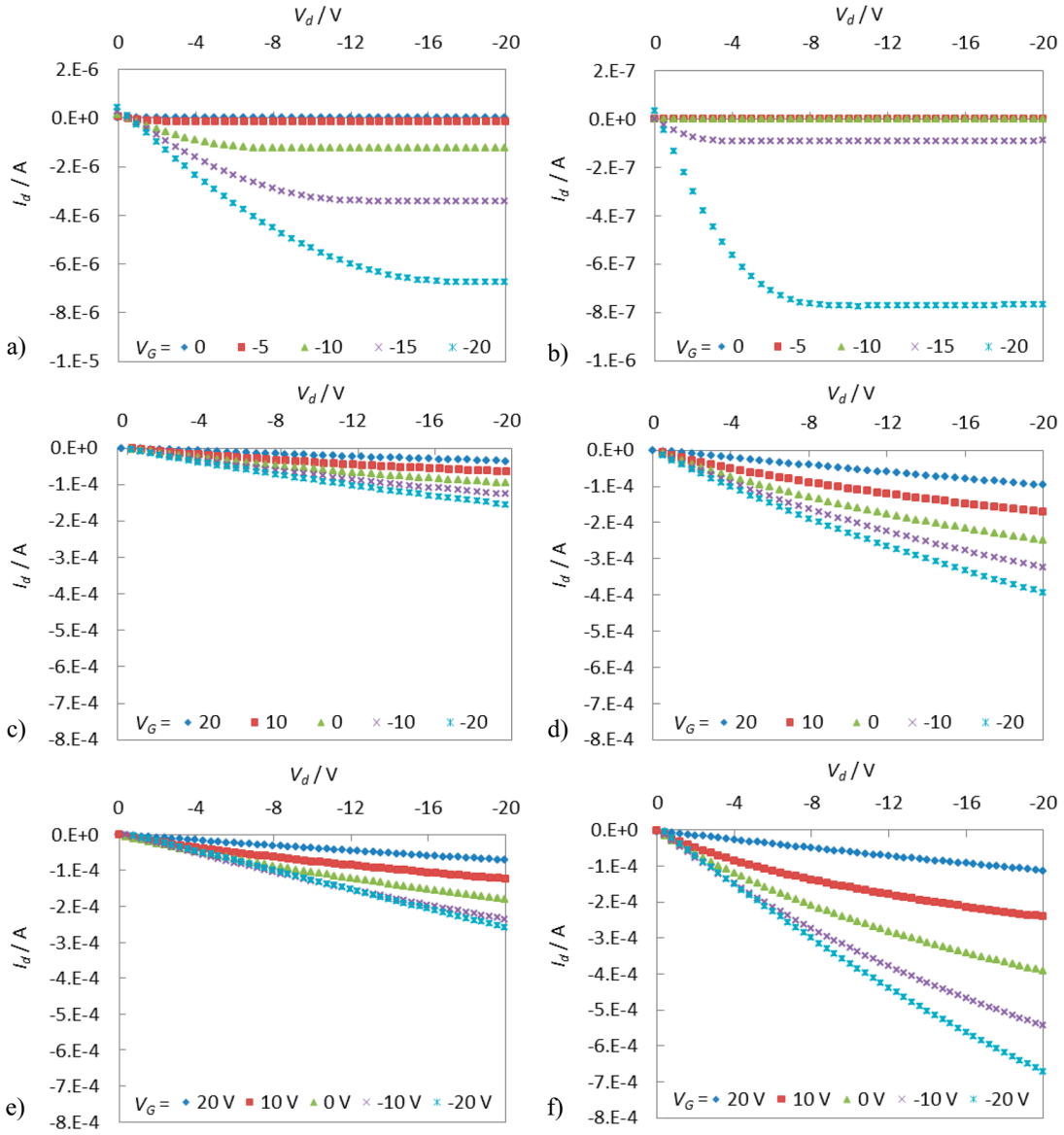

Figure 5. I_d vs V_d plot for (a) 6PTTP6 on PS/SiO_2 and (b) PS+50/SiO_2. (c) Te on PS/SiO_2 and (d) PS+50/SiO_2. (e) Te/6PTTP6 on PS/SiO_2 and (f) PS+50/SiO_2.

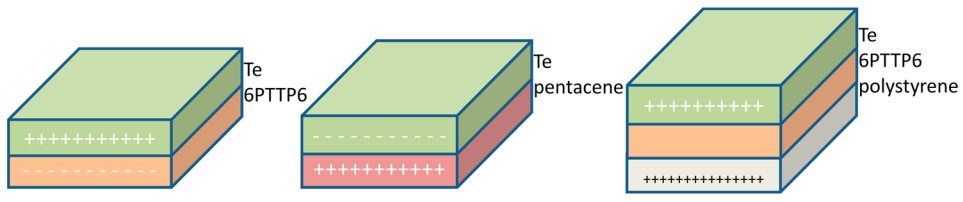

Figure 6. Schematic representation of charge carrier equilibration in bilayers under zero gate voltage. The polystyrene is indicated with embedded static charge.

and defined composition. Here, we have shown that there are chemical and physical methods available to extend the useful V_g range and increase output current in the accumulation mode, including modifying internal fields to alter the V_g-dependent charge distributions and the device regions that determine output currents. More broadly, we illustrate ways in which the essential OFET parameters, generally obtained under DC conditions regardless of the intended applications, are frequency dependent because of the time needed to equilibrate charge distributions with applied fields.

METHODS

Materials. 6PTTP6 was synthesized using a well-established method (ref 19). Pentacene was used as purchased (Sigma Aldrich). Te powder was used as-received (325-mesh, 99.99% metals basis, Alfa Aesar) and is considered to be mildly toxic but has not been reported as carcinogenic. Te vapors were vented from a vacuum chamber into an exhaust system and handled while wearing a dust filter mask. Heavily As-doped silicon wafers (SI-Tech, Process Solutions, $N_D \sim 10^{18}$ cm^3) were cut into 1 in. by 0.5 in. substrates and cleaned by sonication in acetone and 2-propanol for 10 min each and blown dry

dx.doi.org/10.1021/am302221h | ACS Appl. Mater. Interfaces 2013, 5, 1604−1611

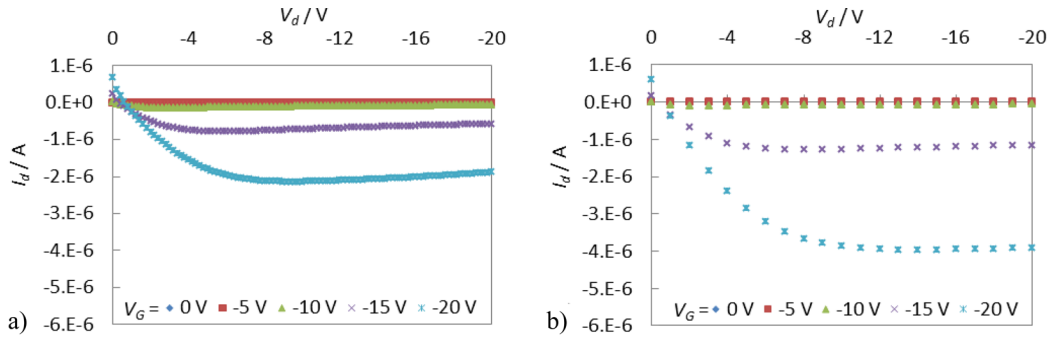

Figure 7. I_d vs V_d plot for (a) Te on heated DR19/SiO_2 with static V_g and (b) V_g pulsed at 1 kHz.

with N_2. The substrates were cleaned further by submerging in piranha solution (sulfuric acid to hydrogen peroxide 3:1, CAUTION: highly corrosive and dangerous to skin) for 20 min, followed by sonication in deionized water for 5 min, blowing with N_2, and baking on a hot plate at 110 °C. The insulator capacitance for 100 nm of thermally grown silicon dioxide is consistent with previous reports, 35 nF/cm^2.

Functionalized DR19 was synthesized as previously reported (ref 25). Monolayers were obtained by dissolving 3 mg in anhydrous toluene (5 mL) in a scintillation vial. Silicon substrates were submerged in the solution and heated to 90 °C for 8 h. Substrates were then rinsed in toluene and THF, respectively, and dried with N_2. Polystyrene (50 000 g/mol, Sigma Aldrich) diluted in toluene (10 mg/mL) was spincoated onto SiO_2 at 1500 rpm and baked for 10 min at 100 °C. Films were embedded with positive or negative charges via corona charging methods described previously (ref 23).

Device Fabrication. FETs were fabricated by thermally evaporating OSC and Te powders using an Edwards thermal evaporation system at base pressures below 3×10^{-6} Torr. Materials were deposited 10 nm thick from alumina crucibles in succession during the same vacuum cycle, using the same deposition rate of 0.3 Å s^{-1}. Si–SiO_2 substrates were held at room temperature during deposition or at 55 °C for comparison. Heated substrates enhance packing of 6PTTP6 molecules (ref 20) and crystallization of Te deposited by thermal evaporation (refs 14 and 17). Gold electrodes were deposited 50 nm thick at 0.5 Å s^{-1} through a shadow mask with 24 electrode pairs, resulting in six devices with each of four W/L ratios (80, 53.3, 40, and 32). All deposition rates and thicknesses were monitored by a quartz crystal microbalance. Substrate temperature was monitored by a thermocouple placed on the backside of substrates. Silicon gates for FETs were accessed by scratching through the oxide with a diamond scribe.

Electrical Measurements. FET measurements were employed using an Agilent 4155C Semiconductor Parameter Analyzer. Low-resistance probes from Micromanipulator were used to test devices under ambient fluorescent lighting conditions, in air, at least 2 h after fabrication. Surface potential measurements were carried out on a Veeco Atomic Force Microscope using a NanoScope IIIa extender and an SCM-PIT tip (Bruker).

■ ASSOCIATED CONTENT

Supporting Information

Table S1 summarizes OFET performance for all additional configurations excluding devices with PS; Table S2 summarizes performances for devices utilizing PS. Figure S1 shows chemical structures; Figure S2 compares morphology of Te on PS uncharged and PS negatively charged; Figure S3 shows morphology of Te and Te/6PTTP6 on PS uncharged versus both on PS positively charged; Figure S4 shows AFM of 6PTTP6 on PS uncharged and PS positively charged. This material is available free of charge via the Internet at http://pubs.acs.org.

■ AUTHOR INFORMATION

Corresponding Author

*E-mail: hekatz@jhu.edu.

Notes

The authors declare no competing financial interest.

■ ACKNOWLEDGMENTS

We thank M. Koontz for assistance with SEM, P. McGuiggan and J. Martinez for assistance with AFM measurements, N. Markovic and O. Alley for assistance with SKPM measurements, and Professor H. Fairbrother for XPS. H.E.K. and R.I. thank the Department of Energy Office of Basic Energy Sciences, Grant Number DE-FG02–07ER46465 (all Te device fabrications, I–V measurements, atomic force microscopy, and manuscript preparation). N.M. and G.J. thank NSF (Division of Electrical, Computer, and Cyber Systems) Grant number ECCS-0823947 for interfacial potential measurements (SKPM). H.E.K., L.Z., and P.G. thank the NSF (Division of Materials Research) MRSEC on Structured Interfaces for DR19 work.

■ REFERENCES

(1) Crone, B.; Dodabalapur, A.; Lin, Y. Y.; Filas, R. W.; Bao, Z.; LaDuca, A.; Sarpeshkar, R.; Katz, H. E.; Li, W. *Nature* **2000**, *403*, 521–523.
(2) Gelinck, G. H.; Huitema, H. E. A.; Van Veenendaal, E.; Cantatore, E.; Schrijnemakers, L.; Van der Putten, J.; Geuns, T. C. T.; Beenhakkers, M.; Giesbers, J. B.; Huisman, B. H.; Meijer, E. J.; Benito, E. M.; Touwslager, F. J.; Marsman, A. W.; Van Rens, B. J. E.; De Leeuw, D. M. *Nat. Mater.* **2004**, *3*, 106–110.
(3) Braga, D.; Horowitz, G. *Adv. Mater.* **2009**, *21*, 1473–1486.
(4) Katz, H. E.; Huang, J. *Thin-Film Org. Elect. Dev.* **2009**, *39*, 71–92.
(5) Kagan, C. R.; Mitzi, D. B.; Dimitrakopoulos, C. D. *Science* **1999**, *286*, 945–947.
(6) Ridley, B. A.; Nivi, B.; Jacobson, J. M. *Science* **1999**, *286*, 746–749.
(7) Pal, B. N.; Dhar, B. M.; See, K. C.; Katz, H. E. *Nat. Mater.* **2010**, *8*, 898–903.
(8) Perez, M. R.; Mejia, I.; Salas-Villasenor, A. L.; Stiegler, H.; Trachtenberg, I.; Gnade, B. E.; Quevedo-Lopez, M. A. *Org. Elect.* **2012**, *13*, 3045–3049.
(9) Ireland, R. M.; Gopalan, P.; Katz, H. E. *Adv. Mater.* **2012**, DOI: 10.1002/adma.201203647.
(10) Dimitrakopoulos, C. D.; Malenfant, P. R. L. *Adv. Mater.* **2002**, *14*, 99–117.
(11) Horowitz, G. *J. Mater. Res.* **2004**, *19*, 1946–1962.
(12) Jung, B. J.; Martinez-Hardigree, J. F.; Dhar, B. M.; Dawidczyk, T. J.; Sun, J.; See, K. C.; Katz, H. E. *ACS Nano* **2011**, *5*, 2723–2734.
(13) Wilson, H. L.; Gutierrez, W. A. *IEEE Lett.* **1967**, 415–416.
(14) Capers, M. J.; White, M. *Thin Solid Films* **1971**, *8*, 353–357.
(15) De Vos, A.; Hindryckx, B. *Proc. IEEE* **1980**, *127*, 42–44.

(16) Torii, H.; Tsuji, M.; Kawaguchi, J. *J. Mater. Res.* **1996**, *11*, 970−980.
(17) Hoffmann, T.; Martinez-Salazar, J.; Herrero, P.; Peterman, J. *Phys. Rev. B* **1997**, *55*, 1858−1863.
(18) Luo, L. B.; Liang, F. X.; Huang, X. L.; Yan, T. X.; Hu, J. G.; Yu, Y. Q.; Wu, C. Y.; Wang, L.; Zhu, Z. F.; Li, Q.; Jie, J. S. *J. Nanopart. Res.* **2012**, *14*, 967.
(19) Tiago, M. L.; Northrup, J. E.; Louie, S. G. *Phys. Rev. B* **2003**, *67*, 115212.
(20) Huang, J.; Sun, J.; Katz, H. E. *Adv. Mater.* **2008**, *20*, 2567−2572.
(21) Huang, J.; Katz, H. E.; West, J. E. *Langmuir* **2007**, *23*, 13223−13231.
(22) Capelli, R.; Toffanin, S.; Generali, G.; Usta, H.; Fachetti, A.; Muccini, M. *Nat. Mater.* **2010**, *9*, 496−503.
(23) Dhar, B. M.; Ozgun, R.; Dawidcyk, T. J.; Andreou, A. G.; Katz, H. E. *Mater. Sci. Eng. R* **2011**, *72*, 49−80.
(24) Dhar, B. M.; Kini, G. S.; Xia, G.; Jung, B. J.; Markovic, N.; Katz, H. E. *Proc. Natl. Acad. Sci. U. S. A.* **2010**, *107*, 3972−3976.
(25) Paoprasert, P.; Park, B.; Kim, H.; Colavita, P.; Hamers, R. J.; Evans, P. G.; Gopalan, P. *Adv. Mater.* **2008**, *20*, 4180−4184.
(26) Vazquez, H.; Gao, W.; Flores, F.; Kahn, A. *Phys. Rev. B* **2005**, *71*, 041306.
(27) Tang, J. X.; Lee, C. S.; Lee, S. T. *J. Appl. Phys.* **2007**, *101*, 064504.
(28) Wang, H.; Yan, D. *NPG Asia Mater.* **2010**, *2*, 69−78.
(29) Braun, S.; Salaneck, W. R.; Fahlman, M. *Adv. Mater.* **2009**, *21*, 1450−1472.
(30) Wang, J.; Wang, H.; Zhang, J.; Yan, X.; Yan, D. *J. Appl. Phys.* **2005**, *97*, 026106.
(31) Zhou, Y.; Fuentes-Hernandez, C.; Shim, J.; Meyer, J.; Giordano, A.; J. Li, H.; Winget, P.; Papadopoulos, T.; Cheun, H.; Kim, J.; Fenoll, M.; Dindar, A.; Haske, W.; Najafabadi, E.; Khan, T. M.; Sojoudi, H.; Barlow, S.; Graham, S.; Bredas, J. L.; Marder, S. R.; Kahn, A.; Kippelen, B. *Science* **2012**, *336*, 327−332.
(32) Greiner, M. T.; Helander, M. G.; Tang, W. M.; Wang, Z. B.; Qui, J.; Lu, Z. H. *Nat. Mater.* **2012**, *11*, 76−81.
(33) Wang, H.; Liu, Z.; Lo, M. F.; Ng, T. W.; Lee, C. S.; Yan, D.; Lee, S. T. *J. Appl. Phys.* **2010**, *107*, 024510.
(34) Dietmueller, R.; Nesswetter, H.; Schoell, S. J.; Sharp, I. D.; Stutzmann, M. *Appl. Mater. Interfaces* **2011**, *3*, 4286−4291.
(35) Ehrler, B.; Wilson, M. W. B.; Rao, A.; Friend, R. H.; Greenham, N. C. *Nano Lett.* **2012**, *12*, 1053−1057.